The 2009 IEEE/RSJ International Conference on
Intelligent Robots and Systems
October 11-15, 2009 St. Louis, USA

Localization for Multi-Axle Train Configured CFMMRs

Andrew Vogt and Mark Minor, *Member, IEEE*

Abstract—**This paper presents a data fusion structure based on comparing geometric configurations of serial connected multi-axle compliant framed robots. Data sources include global odometry derived sources and a novel strain-measurement based Relative Posture Sensor (RPS). Geometric methods are used because stochastic data fusion, developed from prior research, was erroneous when applied to more generalized multi-axle configurations. Our results show an excellent response predicting expected configurations and a reasonable response with un-expected configurations.**

I. Introduction

Compliant Framed wheeled Modular Mobile Robots (CFMMR), shown in **Figure 1**, with a focus on pose estimation, are the subject of this research. These robots use a novel yet simple structure providing suspension and highly controllable steering capability without complex hardware or mechanisms. This is accomplished by coupling axle modules together with a slender flexible frame. The slender geometry caters flexible movement and terrain adaptability by permitting roll and yaw while restricting pitch. Roll provides the robot with suspension capabilities, while yaw allows the robot to easily steer and navigate terrain.

Cooperative robotics poses a unique control problem since it deals with potentially complex interactions between robotic modules. Our prior research successfully established a unique cooperative control architecture to help remedy this problem [1]. This architecture, which is transferrable to cooperative robotic systems on multiple scales, synchronizes kinematic motion controllers, robust dynamic controllers, and sensor fusion methods. Applying these methods to the CFMMR has made it a viable research platform for studying cooperative robotics. Our progressive research is focused on using the CFMMR in a variety of configurations, thus making it more useful for cooperative robotics research. The focus of this paper is to take steps towards generalizing the sensor fusion problem by extending two-axle methods presented in [2] to multi-axle methods.

Building on [2], this paper improves localization through sensor fusion. Effective localization improves drift, lowers antagonistic forces, improves available wheel traction, and ultimately improves the robot's mobility when combined with effective kinematic motion and dynamic control, effective localization. Localization is particularly difficult in compliant robots because nonlinear frame dynamics alter relative poses in unexpected ways. Additionally, many typical operating scenarios, such as planetary exploration, have poor or unavailable global positioning such that dead reckoning is the only alternative. Unfortunately, dead reckoning is frequently derived from odometry which is susceptible to bias and drift.

Our research architecture (Figure 3) builds upon Merrell's foundational Two-Axle data fusion structure [2], called the Relative Measurement Stochastic Posture Error Correction (RMSPEC), which fuses a global dead-reckoning based data source (based on an Extended Kalman Filter) with a Relative Posture Sensor (RPS) [2], robust to bias and drift [3][2]. The RPS consists of strain gauges attached to the compliant frame of the robot, signal processing circuitry, and mathematic algorithms to interpret signals into relative poses. The RPS is simple and lightweight so it can sit on the robot without impeding full range of motion and uses cheap electronics which are resistant to environmental wear.

Our new algorithm, the Geometric Relative Posture Error Correction (GRPEC) algorithm, builds upon RMSPEC to effectively localize multi-axle robots. Extending GRPEC from RMSPEC has seen many challenges resulting from the need to select the most trustworthy axle to become the global reference. Unlike RMSPEC, axle trustworthiness cannot simply be computed relative to the *only* other axle. We explore three methods to effectively localize these axles, of which Method 3 was successful.

Method 1, shown in **Figure 2**, selects the most trustworthy frame followed by selecting the most trustworthy axle of that frame corresponding to RMSPEC deviation metrics. **Figure 2** illustrates this method leads to failure because the belief of

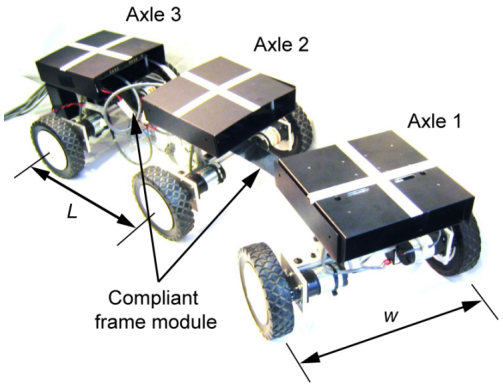

Figure 1: The Serial Connected 3 Axle CFMMR [4]

Manuscript received March 9, 2009. This work was supported in part by NSF Grant No IIS-0308056.

Andrew Vogt is with the Department of Mechanical Engineering, University of Utah, Salt Lake City, UT 84112 USA. (phone: 801-587-9018, e-mail: vogt@eng.utah.edu).

Mark Minor is with the Department of Mechanical Engineering, University of Utah, Salt Lake City, UT 84112 USA. (e-mail: minor@mech.utah.edu).

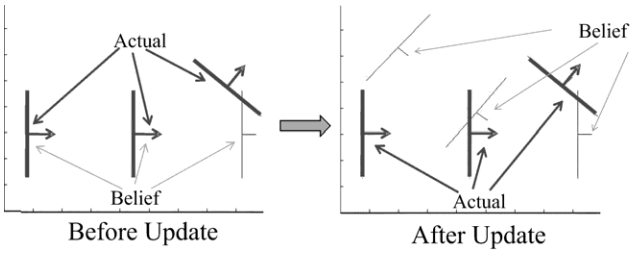

Figure 2: First Candidate Method Using RMSPEC; this doesn't work because the belief does not coincide with the actual configuration after update.

the axles' configurations (thin lines) do not coincide with their actual configurations (thick lines) after the algorithm updates. *Method 2* attempts to correct failures seen from Method 1 by finding trustworthy axles considering the entire robot's geometry. This is accomplished using least squares regression effectively allowing all axles to have a relative degree of trustworthiness. Despite difficulties predicting reasonable configurations this method has significant difficulty converging on a configuration, as shown in **Figure 4** where the error residuals of x and y coordinates never converges (even after 100 iterations).

Our successful *Method 3*, which is illustrated in **Figure 3**, combines identification of trustworthy axles (method one) as they effect the robot's entire geometry (method two). First, global axle poses are derived from odometry (and known initial conditions), while, simultaneously, the RPS relative poses are obtained. Second, odometry derived (OD) and RPS poses are fused to find trustworthy axles using a geometric comparison of axle configurations (GRPEC) opposed to stochastic methods (RMSPEC) thus outputting new poses which are fed back to update OD axle poses. Further, this unique structure may be extended to other cooperative robotic systems including manipulators and distributive sensor networks which are challenged by similar stochastic problems.

The paper is organized as follows: Section II compares relevant contributions from other research, Section III outlines GRPEC's Algorithmic developments, Section IV evaluates our algorithm experimentally, and Section V presents concluding remarks.

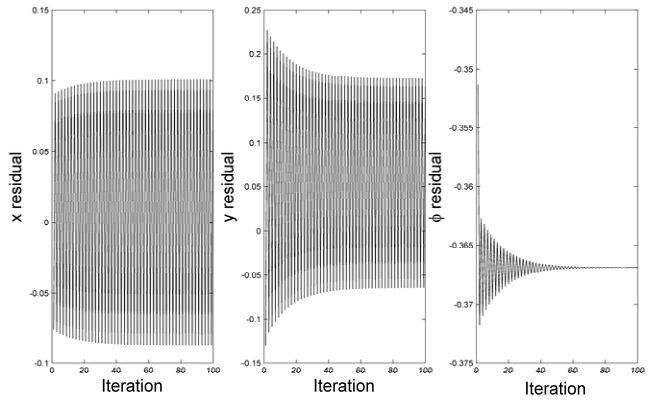

Figure 4: Error Residuals for Least squares method using same configuration as Figure 2; the non converging error shows the robot cannot converge on a configuration.

II. Background

A detailed comparison of the CFMMR with existing robots and vehicles can be found in [5]. Most similar to the structure of the CFMMR is the snake robot Genbu [6] which evolved from early snake robots to provide active wheeled and passive joint morphology for improved terrain adaption and high speed capabilities. Unlike the CFMMR which used a simple and inexpensive compliant frame to connect the axle modules, Genbu connects it's axle modules with complicated and expensive mechanisms. Similar to the RPS, Genbu compliant links are instrumented in order to obtain the axle modules relative positions.

The need for relative position sensing, used in this research, is most similar and highly beneficial to compliant manipulators with large workspaces and limited weight. The resultant links of these manipulators are long and slender resulting in limited stiffness, inherent vibration, significant deflection, and large settling time. Research in this area has been motivated toward controlling the vibrations for fast and precise positioning. Examples include damping out vibrations using strain data [7, 8], accelerometer data [9] and combinations of the two [10] to name a few. Fortunately, the CFMMR's nonholonomic constraints combined with effective inertia and damping of actuators, minimizes problems onset by vibrations. However, both the CFMMR and long-slender manipulators use similar mathematical algorithms to predict relative deflections [2].

Other than strain and mechanism measurement, other non-contact distance measurements can be used to find relative poses [11]. GPS, laser radar, and computer vision are perhaps the most popular alternatives within the robotics community. However, all of these methods are either expensive or incapable of accuracy on our required scale.

The closest found example to our GRPEC data fusion algorithm, besides RMSPEC, is the IPEC algorithm [12]. This algorithm detects the least trustworthy axle, based on odometry, and replaces it with the most trustworthy axle combined with data from a compliant linkage potentiometer.

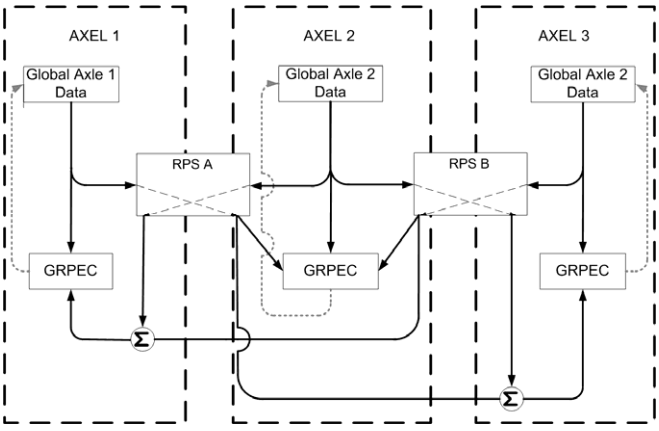

Figure 3: GRPEC's role in axle correction

This method works well, but, like RMSPEC, is not generalized to multiple-serial-axle configurations.

III. GRPEC Algorithm Development

Like both RMSPEC and IPEC, the GRPEC identifies most trustworthy axle, sets it as the global reference, and then updates the other axles by robust relative data with the trustworthy global data. The RMSPEC fuses this data based on data covariance using a covariance intersection (CI) filter. Due to intensified geometric complexity of multiple serial axle configurations, the primary intention of this paper is to design and evaluate the GRMSEC from a high level. This evaluation analyzes snapshot configurations where covariance data is unobtainable, and thus CI filter is unnecessary. By not using the CI filter, we assume RPS data is always more accurate than odometry-derived (OD) data, in the relative reference frame, which is reasonable since strain gauges are less susceptible to environmental disturbances than encoders.

Identifying the most trustworthy axle, thus finding the correct robot configuration is accomplished through minimizing error between global data sets of pure OD data and RPS data *made global* by assigning it an OD global reference. As an example three-axle serial configuration, **Figure 1**, this procedure is conducted for three different scenarios where RPS data is globally attached to either the first, second or third OD axle data and the error is calculated for each of these attachments. This global reference attachment procedure is illustrated with the left-hand-side subfigures of **Figure 5**. The candidate error metrics we consider are position error, orientation error, and deviation angle.

To further illustrate this procedure both data sets (shown by the thin-dashed and thin-solid line types) and their error calculations are shown in the remainder of this section. First, the OD positions and orientations of all axles can be expressed globally as

$$\mathbf{x_{OD}} = \begin{bmatrix} x_{OD1} \\ x_{OD2} \\ x_{OD3} \end{bmatrix}, \mathbf{y_{OD}} = \begin{bmatrix} y_{OD1} \\ y_{OD2} \\ y_{OD3} \end{bmatrix}, \Phi_{\mathbf{OD}} = \begin{bmatrix} \phi_{OD1} \\ \phi_{OD2} \\ \phi_{OD3} \end{bmatrix} \quad (1)$$

where x_{ODi} is the OD horizontal position of the i^{th} axle, y_{ODi} is the OD vertical position of the i^{th} axle, φ_{ODi} is the OD orientation of the i^{th} axle; $\mathbf{x_{OD}}$, $\mathbf{y_{OD}}$, and $\mathbf{\Phi_{OD}}$ are the vector representations of x_{ODi}, y_{ODi}, and φ_{ODi}, respectively, for all axles. There are three relative position/orientation states for frames A and B, respectively, on the robot's expressed as x_{RPSA}, y_{RPSA}, φ_{RPSA}, x_{RPSB}, y_{RPSB}, φ_{RPSB}. Depending on a global reference; to Axle 1, 2, or 3; the relative data can be made global and expressed as

$$\mathbf{x_R} = \begin{bmatrix} x_{R1} \\ x_{R2} \\ x_{R3} \end{bmatrix}, \mathbf{y_R} = \begin{bmatrix} y_{R1} \\ y_{R2} \\ y_{R3} \end{bmatrix}, \Phi_{\mathbf{R}} = \begin{bmatrix} \phi_{R1} \\ \phi_{R2} \\ \phi_{R3} \end{bmatrix} \quad (2)$$

where x_{Ri} is the relative horizontal position of the i^{th} axle, y_{Ri} is the relative vertical position of the i^{th} axle, φ_{Ri} is the relative orientation of the i^{th} axle; $\mathbf{x_R}$, $\mathbf{y_R}$, and $\mathbf{\Phi_R}$ are the vector representations of x_{Ri}, y_{Ri}, and φ_{Ri} respectively. Position errors of each axle are found by computing the norm of the x and y errors

$$\begin{aligned} xy_1Err &= \sqrt{(x_{OD1} - x_{R1})^2 + (y_{OD1} - y_{R1})^2} \\ xy_2Err &= \sqrt{(x_{OD2} - x_{R2})^2 + (y_{OD2} - y_{R2})^2} \\ xy_3Err &= \sqrt{(x_{OD3} - x_{R3})^2 + (y_{OD3} - y_{R3})^2} \end{aligned} \quad (3)$$

where xy_1Err, xy_2Err, and xy_3Err are the composite x and y position errors from Axles 1, 2 and 3, respectively. The orientation errors can be found by taking the absolute value of the difference between global and relative orientation as follows

$$\begin{aligned} \phi_1Err &= |\phi_{OD1} - \phi_{R1}| \\ \phi_2Err &= |\phi_{OD2} - \phi_{R2}| \\ \phi_3Err &= |\phi_{OD3} - \phi_{R3}| \end{aligned} \quad (4)$$

where φ_1Err, φ_2Err, and φ_3Err are the orientation errors of Axles 1, 2, and 3 respectively.

The errors found in (3) and (4) are recalculated for each axle attachment (see **Figure 5**). They are then added for an overall representation of axle trustworthiness as follows:

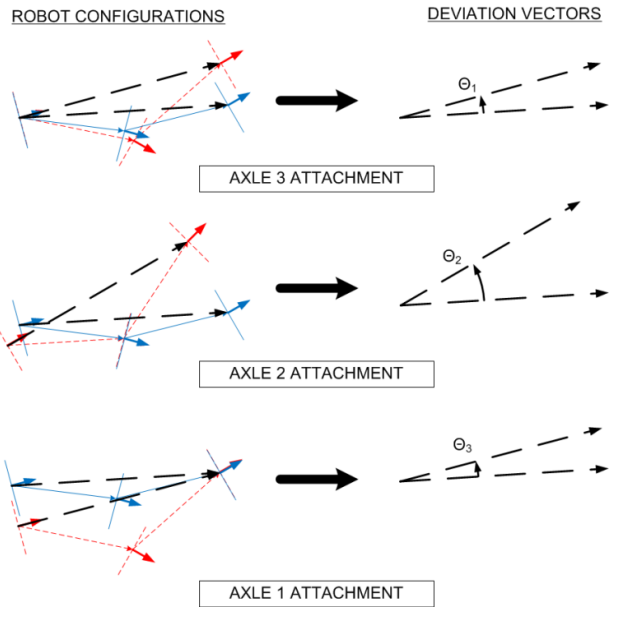

Figure 5: Robot configurations (left-hand-side sub-figs) and deviation vectors (right-hand-side sub figs) for given global (thin-solid line) and relative (thin-dashed line) configurations.

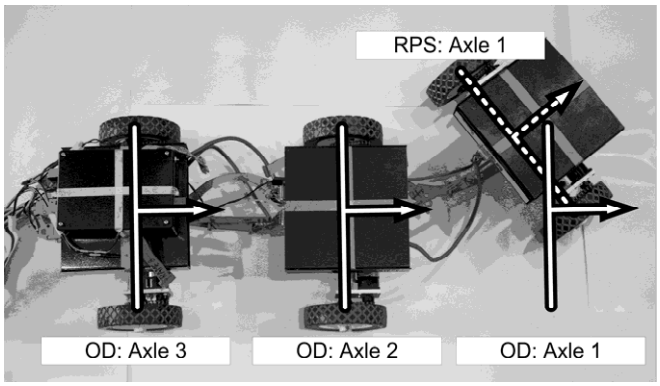

Figure 6: Static Testing procedure of GRPEC using OD and RPS data. The background photo of the robot shows the correct configuration, OD data (white solid lines) shows where the robot initially localizes itself, and RPS (white dashed line) data shows where the robot will be localized if correctly updated.

$$\theta_{xy}^{j} = xy_1 Err + xy_2 Err + xy_3 Err$$
$$\theta_{\phi}^{j} = \phi_1 Err + \phi_2 Err + \phi_3 Err \quad (5)$$

where θ_{xy}^{j} and θ_{ϕ}^{j} are the composite position and orientation errors, respectively, for axle j attachment where j=1, 2, or 3. The most trustworthy axle will also have the lowest composite error.

To define deviation angle, we first define a *pseudo-frame* deviation vector connecting adjacent axles to each other. This is shown in **Figure 5** by the thin linetypes where thin-solid and thin-dashed linetypes represent global OD and RPS data. In the RMSPEC, experimental results showed a smaller angular deviation of these vectors often indicated the most trustworthy axle in the two axle configuration. Therefore, the deviation angle could simply be defined as magnitude of the angle between the two vectors.

Part of the reason this worked in the RMSPEC is because the pseudo-frame vectors also defined the relationship between the endpoints of the robot and reasonably shows deviation of the entire robot. Because these vectors, by themselves, do not connect the beginning to the end of the robot they are incapable of measuring the entire robots deviation and the same metric can not be applied. Instead, a metric which measures the tendency of the entire robot to deviate to applied. This is accomplished by the construction of two new vectors, which represent the *robot-pseudo-frame*, which *only* connects the front to the rear of the robot. This is illustrated by the thick dashed lines in the right-hand-side subfigures of **Figure 5** found by

$$\mathbf{dev_{OD}} = \begin{bmatrix} x_{OD1} - x_{OD3} \\ y_{OD1} - y_{OD3} \end{bmatrix}, \quad and \quad \mathbf{dev_{R}} = \begin{bmatrix} x_{R1} - x_{R3} \\ y_{R1} - y_{R3} \end{bmatrix} \quad (6)$$

where $\mathbf{dev_{OD}}$ and $\mathbf{dev_{R}}$ are the deviation vectors of the global and relative data sets for the three-axle robot. Then, the angle between these vectors is the deviation angle and can be found by

$$\theta_{dev}^{j} = \arccos \frac{\mathbf{dev_{OD}} \cdot \mathbf{dev_{R}}}{\|\mathbf{dev_{OD}}\| \|\mathbf{dev_{R}}\|} \quad (7)$$

Where θ_{dev}^{j} is the deviation angle for axle j attachment where j=1, 2, or 3. Like (5), the most trustworthy axle (j) will also have the minimum θ.

IV. Experimental Evaluation

A. Experimental Methods

For the scope of this paper, evaluation of the preceding error metrics is based on static testing. This testing procedure looks at snapshots of probable configurations, realized through prior research and experience with the CFMMR [1], and compares how well the algorithm converges using the candidate error metrics. The advantage of this procedure is many configurations can quickly be studied, and furthermore, it can be used to more precisely identify the system's failure modes.

This procedure is illustrated by **Figure 6**. The background photograph of the robot shows the actual global configuration of all three axles, the white-solid linetype represents the OD predictions of global states, and the white-dashed linetype represents the correctly predicted global RPS. These two data sources are fused together and then compared to the actual configuration. In our tests, one of the axles is known and assigned as the true global axle. Using our example scenario presented in **Figure 6**, we know either OD data from either Axle 2 or 3 is acceptable because it coincides with the actual global axle as shown in the photograph. To perform quick testing, the actual global poses of the other axles are generated based on RPS data which was confirmed to be accurate (approximately 1-3 cm) relative to the ground truth.

B. Performance Metrics

Experimental Results are presented in Table 1, Table 2, and Figues 5-8. Table 1 illustrates the decision making process of all four representative tests (displayed in Figures 5-8) through using the GRPEC's minimum error selection criteria. For each test, this table provides a brief description of the test, the corresponding error from fitting the RPS-OD globalized data to the actual global reference, the selected global reference based on minimum error (highlighted in gray), and two confidence measures which help evaluate our algorithm's logic. The logic of our algorithm is highly based upon the configuration illustrated in **Figure 6** because it is very clear which axles are most trustworthy. Thus, our confidence measures are catered toward this type of configuration. Confidence measure 1 (CON_1) measures how far the predicted and most erroneous axles are from each other. It is calculated using the following formula

$$CON_1 = \frac{\mathbf{max}(ERR.) - \mathbf{min}(ERR.)}{\mathbf{max}(ERR.)} \quad \rightarrow \quad 0 < CON_1 < 1 \quad (8)$$

where **max**(*ERR.*) and **min**(*ERR.*) are the maximum and minimum axle errors, respectively. This metric quantifies how erroneous the largest error axle is in comparison to the smaller error axle, e.g. as $CON_1 \rightarrow 1$ we gain a high confidence in our update due to the large separation of maximum and minimum errors. Confidence measure 2 (CON_2) measures how close the error of the most trustworthy (lowest error) axle is from the next most trustworthy axle. It is calculated with the following formula

$$CON_2 = \frac{\mathbf{med}(ERR.) - \mathbf{min}(ERR.)}{\mathbf{med}(ERR.)} \quad \rightarrow \quad 0 < CON_2 < 1 \tag{9}$$

where **med**(*ERR.*) is the median error measurement, e.g. as $CON_2 \rightarrow 0$ we gain a greater confidence because this often implies either select the axle associated with **mid**(*ERR.*) or **med**(*ERR.*). Although these confidence measures are useful, they have limitations discussed in the next section.

C. Results and Discussion

Table 2 shows the convergence for each of the four tests. For simplicity, actual data is generated by knowing one of the axle's global poses and applying the RPS to find the other global axle configurations. This is a reasonable procedure because the RPS accurately approximates the actual shape of the robot's frames. This explains why, in TABLE 2, there are errors of zero, signifying a pass (P), opposed to very small numerical errors. A more significant error (such as 0.065 m) signifies a failed (F) configuration.

According to results, all proposed error metrics reasonably identify the most trustworthy axle ultimately leading to the correct configuration. As expected, configurations with the least amount of difficulty converging are those with a *clearly* deviant axle (*test 1* and *4*) which show an excellent response with respect to *both* confidence measures. The other configurations (*test 2* and *3*), were implemented to test how the algorithm responded when the most deviant axle was not as clear. Although these tests show a working architecture, at least with respect to minimization of θ_{xy}, It is important to note failures modes exist for *all* metrics. For example, *test 2* fails when the curvature of both frames are equal and *test 3* fails when the curvature of one of the fames is about 67% of the other frame. These conditions are not presented here because we feel it important to show our algorithm's flexibility with unexpected configurations (*test 2* and *3*)

Because confidence metrics are tailored toward *tests 1* and *4* it is reasonable that their values are not as insightful for *tests 2* and *3*. E.g. it seems clear, based on the θ_{xy}/*test 3* confidence measures for (CON_1=.511 and CON_2=.016), that Axle 2 is correct, but this is certainly not the case for *test 2* where despite CON_2 yielding lower confidence, the correct axle is still selected. Likewise for θ_{dev}/*test 3,* confidence measures (CON_1=.561 and CON_2=.374), particularly CON_2, ensure less confidence in *test 3*. Although this result is desirable, CON_2 produces misleading results signifying future work must be done to further improve our

TABLE 2: ACTUAL POSITION ERROR (IN METERS) RESULTING FROM GRPEC DATA FUSION

TEST	θ_{xy}		θ_{φ}		θ_{dev}	
	ERR	P/F	ERR	P/F	ERR	P/F
1: Fig 5	0	P	0	P	0	P
2: Fig 6	0	P	0	P	0	P
3: Fig 7	0	P	0.065	F	0.065	F
4: Fig 8	0	P	0	P	0	P

TABLE 1: RESULTS OF 4 REPRESENTATIVE STATIC TESTS: FOR EACH TEST, THIS TABLE PROVIDES A BRIEF DESCRIPTION OF EACH TEST, THE CORRESPONDING ERROR FROM FITTING THE RPS TO EACH GLOBAL REFERENCE AND THE SELECTED GLOBAL REFERENCE BASED ON MINIMUM ERROR (HIGHLIGHTED IN GRAY)

TEST	DESCRIPTION	axel *j*	θ_{xy}			θ_{φ}			θ_{dev}		
			AX. ERR. (m)	CON_1	CON_2	AX. ERR. (deg)	CON_1	CON_2	AX. ERR. (deg)	CON_1	CON_2
1: Fig 5	**RPS_A** → pure bend; **RPS_B** → no bend; **Encoder-data** →aligned	axle 1	0.357	0.622	0.022	68.4	0.498	0.008	23.0	0.519	0.024
		axle 2	0.138			34.6			11.3		
		axle 3	0.135			34.3			11.1		
2: Fig 6	**RPS_A** → pure bend; **RPS_B** → pure bend w/ ≠ κ; **Encoder-data** → aligned	axle 1	0.758	0.635	0.491	151.9	0.400	0.250	52.3	0.838	0.782
		axle 2	0.277			91.2			8.5		
		axle 3	0.544			121.5			38.8		
3: Fig 7	**RPS_A** → pure bend; **RPS_B** → pure bend w/ ≠ κ & opposite sign; **Encoder-data** → aligned	axle 1	0.305	0.511	0.016	60.8	0.401	0.248	15.7	0.561	0.374
		axle 2	0.300			101.5			25.0		
		axle 3	0.613			80.8			35.7		
4: Fig 8	**RPS_A** → no bend; **RPS_B** → no bend; **Encoder-data** → axel 1 simulates pure bending	axle 1	0.608	0.630	0.013	120.8	0.499	0.005	41.8	0.559	0.015
		axle 2	0.225			60.6			18.4		
		axle 3	0.228			60.8			18.7		

understanding of confidence metrics for a wider range of configurations

Additional future work will improve these results through implementation of advanced data fusion techniques on both the axle level, using Extended Kalman Filters (EKF), and the frame level by using Covariance Intersection (CI) filter (similar to methods used in the original RMSEPC). Also, we will focus on testing these algorithms under realistic dynamic conditions and more generalized configurations.

V. Conclusion

This paper explored geometric based localization techniques in Multi-Axle Compliant Framed Modular Mobile Robots. The proposed algorithms show successful implementation of these algorithms on a high level and for generalized configurations. Future work will extend these algorithms to more generalized configurations and test them using dynamic operating conditions.

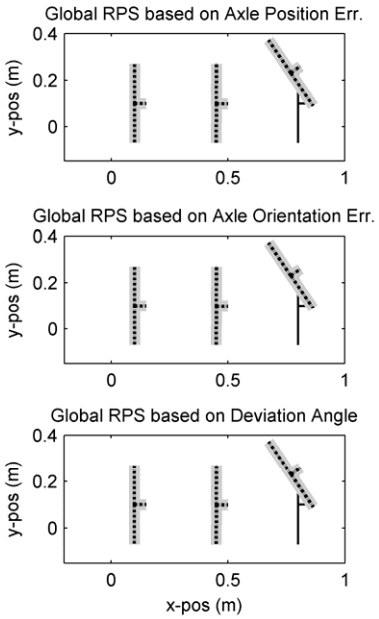

Figure 7: OD axles located at x=[.8 .45 .1]T, y=[.1 .1 .1], φ=[0 0 0] while the front RPS axle is in pure bending.

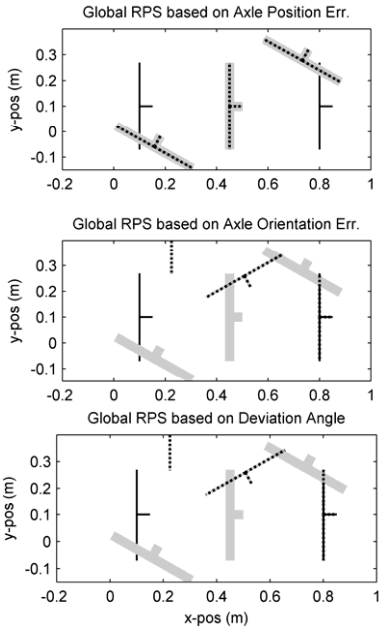

Figure 8: OD axles located at x=[.8 .45 .1]T, y=[.1 .1 .1], φ=[0 0 0] while the front and rear frame in pure bending of opposite sign but unequal magnitude

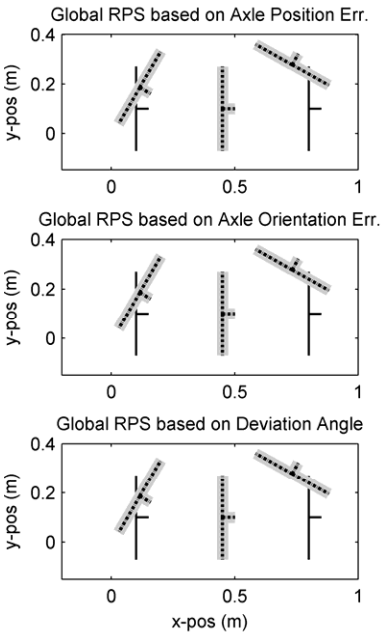

Figure 9: OD axles located at x=[.8 .45 .1]T, y=[.1 .1 .1], φ=[0 0 0] while the front and rear frame in pure bending of same sign but unequal magnitude

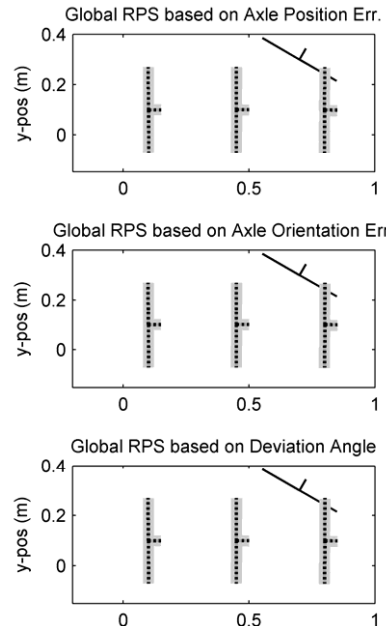

Figure 10: OD axles located at x=[.7 .45 .1]T, y=[.3 .1 .1], φ=[π/3 0 0] while both RPS frames are straight.

References

1. **Zhu, X., et al., *Cooperative motion control and sensing architecture in compliant framed modular mobile robots.* IEEE Transactions on Robotics, 2007. 23(5): p. 1095-1101.**
2. **Minor, M.A., and Merrell, R., Instrumentation and Algorithms for Posture Estimation in Compliant Framed Modular Mobile Robots. The International Journal of Robotics Reserach, 2007. 26: p. 491-512.**
3. **Merrell, R., and Minor, M.A., Internal posture sensing for a flexible frame modular mobile robot, in IEEE International Conference on Robotics and Automation. 2003: Taipei, Taiwan.**
4. **Kim, Y. and M.A. Minor. Decentralized kinematic motion control for multiple axle compliant framed modular wheeled mobile robots. 2006. Piscataway, NJ 08855-1331, United States: Institute of Electrical and Electronics Engineers Inc.**
5. **Minor, M.A., Albiston, B.W. and Schwensen, C.L., Simplified motion control of a two axle compliant framed wheeled mobile robot. IEEE Transactions on Robotics, 2006. 22(3): p. 491-506.**
6. **Kimura, H., and Hirose, S., Development of Genbu: Active wheel passibe joint articulated mobile robot, in IEEE/RSJ IROS 02 Proceedings. 2002: Lausanne, Switzerland.**
7. **Carusone, J., K.S. Buchan, and G.M.T. D'Eleuterio, Experiments in end-effector tracking control for structurally flexible space manipulators. IEEE Transactions on Robotics and Automation, 1993. 9(5): p. 553-560.**
8. **Ge, S.S., T.H. Lee, and G. Zhu, Improving regulation of a single-link flexible manipulator with strain feedback. IEEE Transactions on Robotics and Automation, 1998. 14(1): p. 179-85.**
9. **Kotnik, P.T., S. Yurkovich, and U. Ozguner. Acceleration Feedback Control For A Flexible Manipulator Arm. 1988. New York, NY, USA: IEEE.**
10. **Khorrami, F. and S. Zheng. Vibration control of flexible-link manipulators. 1990. Green Valley, AZ, USA: American Autom. Control Council.**
11. **DeSilva, C.W., Mechatronics: An Integrated Approach 2004, Boca Raton/London/New York/Washinton D.C.: CRC Press.**
12. **Borenstien, J., Experimental results from internal odometry error correction with the OmniMate mobile robot. IEEE Transactions on Robotics and Automation, 1998. 12(4): p. 257-273.**